ELSEVIER

Nuclear Instruments and Methods in Physics Research A 415 (1998) 85–92

NUCLEAR INSTRUMENTS & METHODS IN PHYSICS RESEARCH Section A

On possible target design for a heavy ion ignition facility

M. Basko[a,*,1], K.-J. Lutz[b], J. Maruhn[b]

[a] *Institute for Theoretical and Experimental Physics, B. Cheremushkinskaya 25, Moscow 117259, Russian Federation*
[b] *Institut für Theoretische Physik, Universität Frankfurt, P.O. Box 111932, 60054 Frankfurt, Germany*

Abstract

We investigate minimum energy requirements for ignition of indirect drive targets driven by beams of heavy ions. Two types of hohlraums containing an NIF-scale fusion capsule [J. Lindl, Phys. Plasmas 2 (1995) 3933] are considered. The required ion beam energy is evaluated by combining two and three-dimensional view factor simulations of the radiation transport with one-dimensional hydrodynamic simulations of the converter dynamics. It is found that an ignition facility based on the HIDIF driver concept (I. Hofmann, Nucl. Instr. and Meth. 1998) would require about 4 MJ of the ion beam energy. The impact of the ion-range shortening on target performance is discussed in some detail.

PACS: 52.58.Hm; 52.40.Mj

Keywords: Heavy ion inertial fusion

1. Introduction

One of the key issues for heavy ion inertial fusion is to meet requirements of the target physics with constraints imposed by the driver. In this work we investigate indirect drive target options that could match the driver scheme of the HIDIF study [1,2], which is based on an RF linear accelerator with a number of storage rings and a vacuum ballistic focusing system. Our main goal is to evaluate the minimum amount of the ion beam energy E_b required for ignition.

An indirect drive target consists of a spherical fusion capsule placed in the center of a radiation cavity – a hohlraum. Here we do not simulate the capsule performance but rather take advantage of the experience accumulated in the Livermore laser fusion programme and adopt the NIF capsule [3,4] as the smallest one for which ignition is still feasible. Then, the enclosure of the fusion capsule is designed in such a way as to meet the specific requirements of the heavy ion driver.

The principal constraints given by the HIDIF study [2] which affect most directly the required total beam energy E_b are the energy of the beam ions, $\varepsilon_{bi} \geq 10\,\text{GeV}$ per nucleus of $A \simeq 200$, and the focal spot size on the target, $r_{foc} \geq 1.5\,\text{mm}$. For a given target configuration, these two restrictions

* Corresponding author. E-mail: basko@vitep5.itep.ru.

[1] Partially supported by GSI, Darmstadt, Germany.

0168-9002/98/$19.00
PII: S0168-9002(98)00372-6

set a lower limit for the total mass of the converter material,

$$M_{\mathrm{con}} = N_{\mathrm{con}} \cdot \langle \rho l \rangle_{\mathrm{bi}} \cdot \pi r_{\mathrm{foc}}^2, \quad (1)$$

which is to be heated to a temperature of some 300 eV; here N_{con} is the number of X-ray converters, and $\langle \rho l \rangle_{\mathrm{bi}}$ [g/cm^2] is the range of the beam ions. The energy spent to heat up the converter mass constitutes one of the major loss terms in the energy balance of the targets considered below.

Among other things, ignition of the NIF capsule requires a delicate pulse shaping of the driving power [3,5]. Here, being interested primarily in minimizing the driver energy, we forgo any discussion of the pulse shaping problem and adopt a simple approximation to the NIF pulse profile which, to our understanding, must be adequate for evaluating the overall target energetics and the symmetry of the X-ray drive on the fusion capsule.

2. Hohlraum design and target dimensions

We assume that the fusion capsule has a fixed outer radius of $R_{\mathrm{c}} = 1.1$ mm and needs to absorb 150 kJ of thermal X-ray energy to be ignited. The latter values correspond approximately to the lower bound of the NIF baseline capsule designs [3]. For a given fusion capsule, the hohlraum geometry has to be chosen such as (i) to provide the necessary uniformity of the X-ray drive on capsule, (ii) to maximize the energy coupling efficiency between the ions and the fusion capsule, and (iii) to satisfy the constraints imposed by the ion beam transport and final focusing systems. We analyze and compare two different hohlraum configurations dubbed as "octopus" and "lemon" targets and shown respectively in Figs. 1 and 2.

The "octopus" target depicted in Fig. 1 has a three-dimensional (3-D) geometry. It is composed of a cylindrical hohlraum case which is irradiated by eight clusters of ion beams impinging on eight X-ray converters placed symmetrically (four above and four below) with respect to the horizontal midplane. In practice, the upper four converters can be rotated azimuthally with respect to the four lower ones by a certain angle. The vertical position of the converters and the waist radius of the hohlraum are chosen so as to bring the amplitudes of the lower asymmetry modes on the fusion capsule below 1%. This target has no radiation screens inside the hohlraum, which makes the overall design simpler and less sensitive to fabrication and positioning errors. The converter material is imbedded into tube-like pockets to confine its expansion as close to one-dimensional (1-D) flow as possible. The depth of the converter pockets is chosen such that during the main pulse the front edge of the ion penetration depth sticks out into the hohlraum by no more than $\simeq 0.5$ mm.

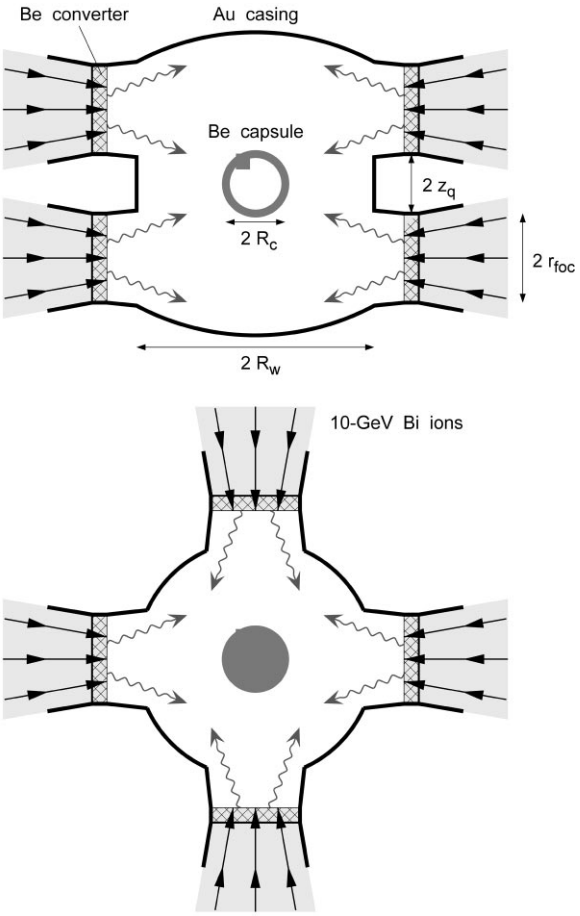

Fig. 1. Cut-away front and top views of the "octopus" target with eight X-ray converters and no radiation screens. Above: vertical (meridional) cross-section through the centers of diametrically opposite converters. Below: horizontal cross-section through the upper tier of four converters.

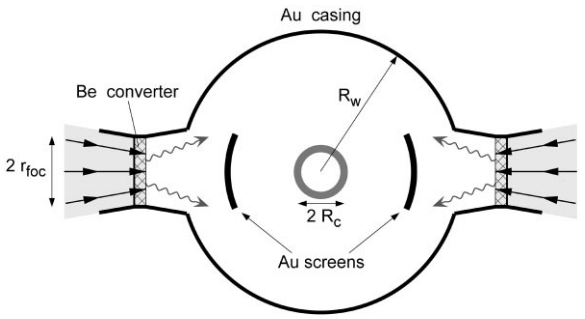

Fig. 2. Meridional cross-section of the "lemon" target with two X-ray converters irradiated by ion beams from two sides. This target is rotationally symmetric with respect to the horizontal axis and has two radiation screens.

The "lemon" target shown in Fig. 2 is rotationally symmetric with respect to the horizontal axis. It is irradiated from two sides and, correspondingly, has only two X-ray converters. This target design ascends to earlier publications by the Livermore group [3]. It has two radiation shields, whose size and position are adjusted so as to suppress the $l = 2$ asymmetry mode of the X-ray drive on the fusion capsule and maximize the energy delivered into it. The radius of the hohlraum case is chosen so as to bring the $l = 4$ asymmetry mode down to $< 1\%$.

3. View factor results for symmetry and X-ray energy

The hohlraum energy coupling efficiency and the symmetry of the X-ray drive have been evaluated by performing static view factor simulations. The view factor codes VF2 [6] and HOLCON [7] have been used, respectively, for the 2-D (two-dimensional) and 3-D simulations. In these simulations no converter material was present in the hohlraum, and the X-ray energy was injected at imaginary surfaces adjacent to the side and end walls of the converter pockets. The X-ray power pulse was tailored to imitate the main features of the NIF pulse [3]

$$W_x(t) = \begin{cases} \delta_x W_{x0}, & 0 < t < t_1, \\ \delta_x W_{x0}\ \exp\left(\dfrac{t - t_1}{\Delta t_{12}}\right), & t_1 < t < t_2, \\ W_{x0}, & t_2 < t < t_3. \end{cases} \quad (2)$$

Here $\delta_x = 0.02$, $t_1 = 10\,\text{ns}$, $t_2 = 15\,\text{ns}$, $t_3 = 17\,\text{ns}$, and $\Delta t_{12} = (t_2 - t_1)/\ln \delta_x^{-1}$. The peak power W_{x0} was adjusted in each particular case so as to allow the fusion capsule absorb 150 kJ of the X-ray energy.

Table 1 presents the results of the 2-D simulations of the "octopus" hohlraum for three different values of the focal spot radius r_{foc} and two values of the hohlraum case size, namely $R_w = 4R_c$ and $R_w = 3R_c$. The hohlraum with $R_w = 4R_c$ represents the base case of our study. As it is seen in Fig. 3a, this hohlraum proportion ensures a good symmetry of the X-ray drive on the fusion capsule: after some 3 ns the peak-to-valley (ptv) non-uniformity amplitude of the X-ray flux drops to $< 1\%$, and stays at this level afterwards. Fig. 3b shows that, once the elevation z_q of the converter pockets above the midplane has been adjusted to minimize the $l = 2$ mode, the dominant asymmetry component remains in the $l = 4$ Legendre harmonic.

When performing the 2-D simulations of the 3-D "octopus" hohlraum, the latter was reduced to a 2-D rotationally symmetric configuration whose meridional cut coincides with the top view in Fig. 1 (the axis of rotation is along the vertical). Clearly, such a reduction cannot be done in a physically equivalent way with respect to all parameters. Hence, for each 3-D case we performed two 2-D runs to obtain an upper and a lower bound for the total X-ray energy $E_x = \int_0^{\infty} W_x(t)\,dt$ required for ignition: in the first run we preserved the depth of the converter pockets, in the second one we preserved the total surface area of the hohlraum case. As

Table 1
Energy required to ignite the "octopus" target depicted in Fig. 1 at three different values of the beam focus radius r_{foc}

	r_{foc} (mm)		
	0.66	1.1	1.65
$R_w = 4R_c$			
S_{con} (mm^2)	11	30.4	68.4
E_x (MJ)	1.3 ± 0.2	1.4 ± 0.2	1.55 ± 0.1
E_b (MJ)	2.2 ± 0.2	2.9 ± 0.2	4.1 ± 0.1
$R_w = 3R_c$			
E_x (MJ)	1.0 ± 0.2	1.05 ± 0.15	1.1 ± 0.15
E_b (MJ)	1.8 ± 0.2	2.4 ± 0.1	3.4 ± 0.1

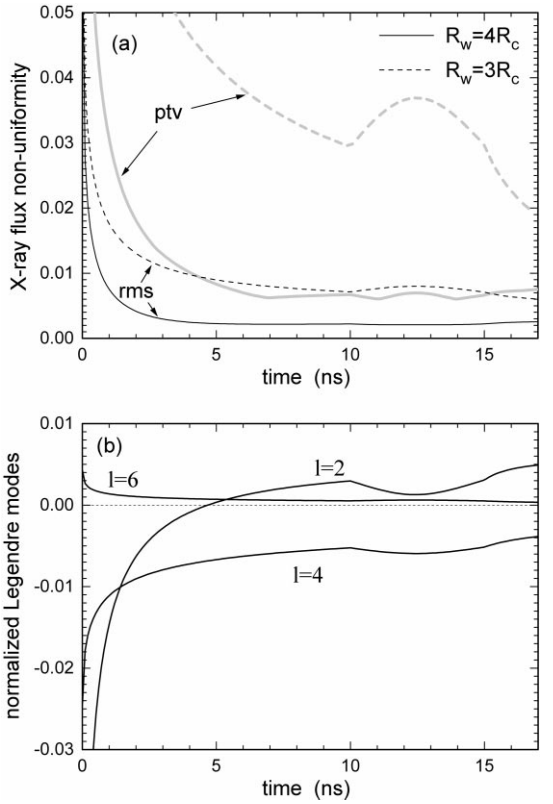

Fig. 3. (a) Temporal variation of the peak-to-valley (ptv) and root-mean-square (rms) non-uniformity amplitudes of the X-ray flux on the fusion capsule in the "octopus" target as calculated with the 2-D view factor code VF2 for two values of the hohlraum case radius R_w. (b) Normalized amplitudes of the three lowest non-vanishing Legendre harmonics for the same flux non-uniformity.

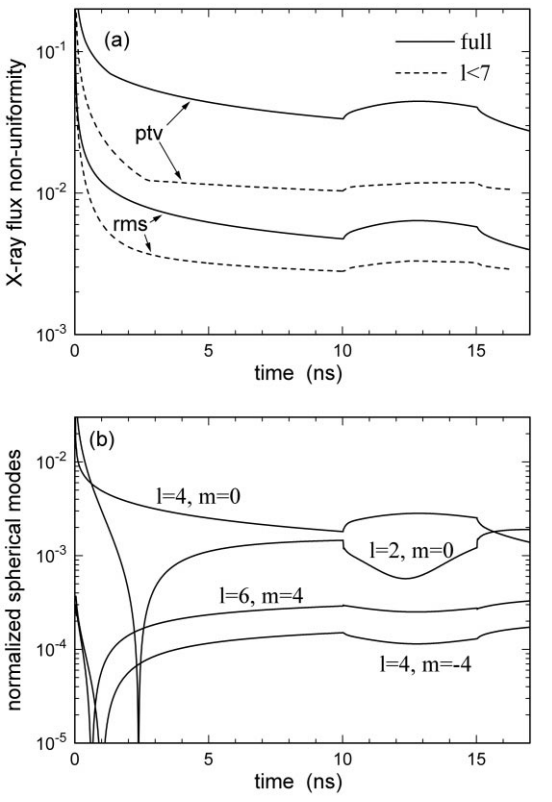

Fig. 4. (a) The same as in Fig. 3a but calculated with the 3-D view factor code HOLCON for $R_w = 4R_c$. Solid: full amplitudes obtained from the actual flux variations. Dashed: amplitudes obtained by summing up the contributions of the $l \leq 6$ angular modes only. (b) Normalized amplitudes of the four lowest spherical modes with the highest contributions to the 3-D flux non-uniformity.

a result, Table 1 lists the mean values of E_x, with the "error bars" indicating half of the difference between thus obtained upper and lower bounds. From Table 1 one sees that the "octopus" target with an acceptable non-uniformity level of the X-ray drive (ptv $<1\%$) requires some 1.3–1.6 MJ of the X-ray energy to be generated in the hohlraum.

The 3-D view factor simulations of the "octopus" hohlraum have been done for the base case of $r_{foc} = 1.65\,\text{mm}$, $R_w = 4R_c$ only. Fig. 4 shows the corresponding results for the symmetry of the X-ray drive. The problem with the 3-D simulations is a relatively high level of numerical noise in high-order angular modes. As it is seen in Fig. 4a, the ptv and rms (root-mean-square) amplitudes calculated by summing up the contributions of only $l \leq 6$ spherical harmonics are in good agreement with the 2-D results (shown in Fig. 3a), but fall a factor 2–3 below the full amplitudes calculated by comparing the flux values in all the individual mesh zones. Since there are no physical reasons why a relatively spacious "octopus" hohlraum would generate a significant ($>1\%$) asymmetry in the $l \geq 7$ modes (which is confirmed by the 2-D results), we conclude that the true 3-D asymmetry must be close to that represented by the dashed $l < 7$ curves in Fig. 4a, i.e. around 1% for the ptv amplitude.

Fig. 4b shows the amplitudes $|a_{lm}|$ of the strongest spherical modes normalized to $a_{00} = 1$. Such a normalization implies that in the pure 2-D case the same asymmetry is represented by the values of a_{l0} a factor $\sqrt{2l+1}$ smaller than the normalized amplitudes c_l of the Legendre modes shown in Fig. 3b. With the account for this renormalization factor, the 3-D mode $l = 4, m = 0$ of Fig. 4b agrees well with the $l = 4$ 2-D mode in Fig. 3b. It is also seen that the strongest azimuthal modes with $m = \pm 4$ (not captured in the 2-D simulations), which arise from the four-sided irradiation pattern, are well below the meridional mode $l = 4, m = 0$. The latter can be explained by a relatively large size of emitting spots inside the cylindrically symmetric hohlraum. The total required X-ray energy, $E_x = 1.6\,\mathrm{MJ}$, calculated with the 3-D code, is also within the "error bars" of the 2-D simulations.

To illustrate how the efficiency of the "octopus" hohlraum can be improved by reducing the case-to-capsule area ratio, we have performed also 2-D simulations for a smaller hohlraum size of $R_\mathrm{w} = 3R_\mathrm{c}$. It is seen from Table 1 that such a tighter hohlraum saves about 0.3–0.5 MJ of the X-ray energy, which brings the required driver energy down by some 0.5–0.7 MJ. The penalty is a sharp increase in the non-uniformity of the X-ray drive to an unacceptable level of $\simeq 2.8\%$ (time-integrated) in the $l = 4$ mode. The temporal behavior of the $l = 2$ and $l = 4$ modes in this case is similar to that shown in Fig. 3b. As a possible remedy, one might consider an appropriate "shimming" of the fusion capsule to neutralize the $l = 4$ asymmetry, but the feasibility of this approach remains so far rather uncertain.

The results of the 2-D simulations for the "lemon" target are given in Table 2. The size and position of the two radiation screens have been adjusted such as (i) to suppress the $l = 2$ asymmetry mode, and (ii) to maximize the energy transfer into the capsule. The radius of the hohlraum case, $R_\mathrm{w} = 6R_\mathrm{c}$, is chosen so as to obtain the same (not higher) amplitude (0.6%) of the time-integrated $l = 4$ asymmetry mode as in the base case of the "octopus" target. The resulting value of the required X-ray energy, $E_x = 2.2\,\mathrm{MJ}$, when compared with the $E_x \leq 1.6\,\mathrm{MJ}$ for the "octopus" target, demonstrates a relative inefficiency of the "lemon" hohlraum. This is due to the fact that the radiation screens pose too strong a hindrance to thermal X-rays on their way to the capsule.

Finally, a few remarks on the adequacy of the static view factor simulations. In the relatively spacious "octopus" hohlraum without radiation screens the main consequence of the wall motion for the radiation transport should be a time-dependent effective surface area ratio between the hohlraum case and the capsule. Here the static view factor results, when expressed in terms of the X-ray energy E_x needed to ensure a certain level of the implosion symmetry, are expected to be close to reality. In other words, if, due to the wall motion, one has to start with a larger hohlraum to obtain the same level of the time-integrated asymmetry, the energy penalty during the early phase of the pulse is expected to be roughly reimbursed by the end of the pulse. More questionable is the case of the "lemon" target because expanding radiation screens perturb the initial shading pattern and tend to plug the radiation channels. But even in this case, because the most dangerous $l = 4$ asymmetry mode is controlled by increasing the hohlraum size, we expect the static calculations to be reasonably accurate for the energy-versus-symmetry results (closing of the radiation channels can be alleviated by low-Z lining). Note that the expanding converter material that would spill out of the converter pockets is not expected to radiate energy because of the ion range shortening (see Section 5).

4. Converter dynamics and the driver energy

Once the expansion of the X-ray converters has largely been confined to a 1-D flow, one can use a 1-D radiation-hydrodynamics code to calculate the amount of the ion beam energy E_b needed to generate the X-ray energy E_x calculated above. The structure of the plane-parallel target used for these simulations is shown in Fig. 5. The converter is represented by a 0.5 mm thick layer of solid density beryllium, covered with a thin gold film. As it was discussed in Refs. [8,9], beryllium doped with a small amount of high-Z element would be the optimum material for an X-ray converter heated to a "working" temperature of $\simeq 300\,\mathrm{eV}$. For the

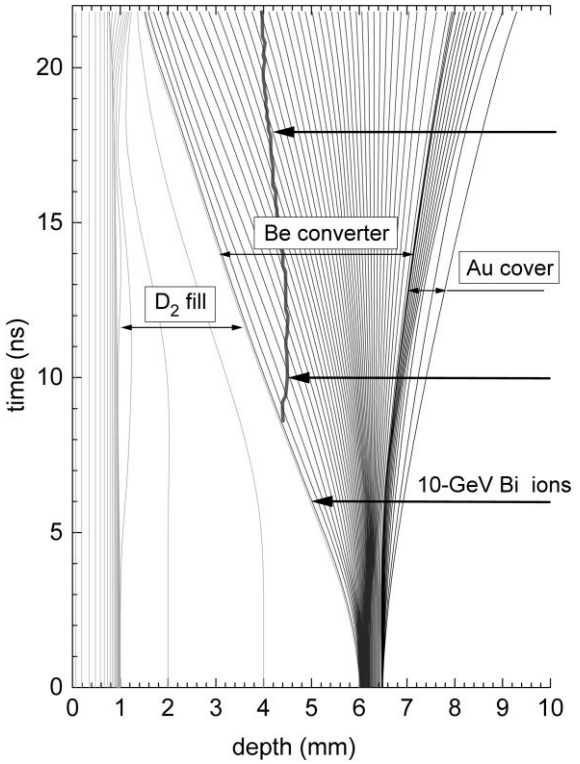

Fig. 5. Space–time diagram of the converter dynamics in the 1-D 3-T hydrodynamic simulations. Initially the beryllium converter ($6.0\,\text{mm} < x < 6.48\,\text{mm}$, $\rho_0 = 1.9\,\text{g/cm}^3$) is covered by a 15 μm layer of solid gold ($\rho_0 = 19.5\,\text{g/cm}^3$). 10 GeV Bi ions enter the target from the right. Central layer ($0 < x < 1\,\text{mm}$) with the equation of state of beryllium simulates an energy sink for the X-rays emerging from the beryllium converter and is excluded from interaction with the Bi ions. Thick solid ragged curve indicates the penetration depth of the Bi ions.

beam parameters studied here, the optimum thickness of the converter cover is close to 15 μm of solid density gold, and this latter value was used in all the simulations discussed below. The hydrodynamic simulations have been performed with the 1-D three-temperature (3-T) code DEIRA [10], which includes a detailed model for the stopping of 10 GeV ^{209}Bi ions in a plasma.

In the 1-D planar geometry all the energies are measured per unit surface area. We, however, quote the full energy values, assuming for simplicity that our planar target has the same surface area,

$$S_{\text{con}} = N_{\text{con}} \pi r_{\text{foc}}^2, \tag{3}$$

as the summed cross section of all the N_{con} converters in the hohlraum. The values of S_{con} are listed in Tables 1 and 2. Note that numerically they roughly coincide with the total beryllium mass in mg because the range of 10 GeV Bi ions in Be is close to $1\,\text{mg/mm}^2$ (see the next section). The temporal profile of the total beam power is similar to that given by Eq. (2), with the only difference that it is preceded by an additional 5 ns long prepulse at twice the foot power to "warm up" the converter. The peak beam power was adjusted so as to have the total X-ray energy which escapes the converter to be equal to $E_{\text{x}} - E_{\text{cw}}$. Here E_{cw} is the energy absorbed by the hohlraum wall across the summed beam cross-section as calculated with the view factor code; it is deducted from E_{x} in order not to be counted twice.

The calculated values of the ion beam energy E_{b} required for ignition of the "octopus" and "lemon" targets are listed in Tables 1 and 2. From Table 1 it is seen that the ignition threshold of the "octopus" target is rather sensitive to the value of the focal spot radius r_{foc} because a large portion of the beam energy is spent to heat up the converters. For $r_{\text{foc}} \gtrsim 1.1\,\text{mm}$ the X-ray conversion efficiency drops below 50%. If we want to meet the "robust" choice of the hohlraum proportion, $R_{\text{w}} = 4R_{\text{c}}$, with the HIDIF constraint on the focal spot radius, $r_{\text{foc}} \geq 1.5\,\text{mm}$, we obtain an ignition threshold of $E_{\text{b}} \approx 4\,\text{MJ}$.

Because the "lemon" target has only two converters, it requires considerably less converter material than the "octopus" target. As a consequence, its ignition threshold becomes lower than that of the "octopus" target at large focal radii, $r_{\text{foc}} > 1\,\text{mm}$, and amounts to 3.6 MJ for the HIDIF value $r_{\text{foc}} = 1.65\,\text{mm}$. It should be noted, however, that there are likely to be additional energy losses (not

Table 2
Energy required to ignite the "lemon" target depicted in Fig. 2 at two different values of the beam focus radius r_{foc}

r_{foc} (mm)	1.1	1.65
S_{con} (mm^2)	7.60	17.11
E_{x} (MJ)	2.2	2.2
E_{dr} (MJ)	3.1	3.6

accounted for in the present simulations) associated with the two-sided irradiation due to the fact that each converter has to accept a large number of individual ion beams spread over a wide range of incidence angles.

5. Role of the ion range shortening

As the stopping material is heated and gets ionized, the mass range of irradiating ions decreases. In our case, the full ion range,

$$\langle \rho l \rangle = \langle \rho l \rangle_{\mathrm{cw}} + \langle \rho l \rangle_{\mathrm{con}}, \tag{4}$$

can be written as a sum of ranges in the gold cover wall, $\langle \rho l \rangle_{\mathrm{cw}}$, and in the converter, $\langle \rho l \rangle_{\mathrm{con}}$. When the hydrodynamic expansion is confined to a planar flow, the quantity $\langle \rho l \rangle_{\mathrm{cw}}$ remains constant, and it is the value of $\langle \rho l \rangle_{\mathrm{con}}$ which is of primary interest for the target design. With the stopping power given by the general expression [11]

$$-\frac{\mathrm{d}\varepsilon_{\mathrm{bi}}}{\mathrm{d}x} = \frac{4\pi\ e^4}{m_{\mathrm{e}}\ v_{\mathrm{bi}}^2} n_{\mathrm{e}} Z_{\mathrm{eff}}^2 L, \quad L = \ln\frac{2m_{\mathrm{e}}\ v_{\mathrm{bi}}^2}{I}, \tag{5}$$

one can identify three physical effects which cause $\langle \rho l \rangle_{\mathrm{con}}$ to shorten as the converter and its cover wall transform into a plasma state:

1. the increase of the Coulomb logarithm L of the converter material due to its ionization,
2. the enhanced non-equilibrium effective charge Z_{eff} of the fast ions in low density plasmas as compared to that in cold metals [12],
3. the increase in the stopping power of the heated and expanding cover wall.

The first effect is easy to evaluate analytically by replacing the mean ionization energy $I = 64\,\mathrm{eV}$ of cold beryllium [11] with the plasmon energy $\hbar\omega_{\mathrm{p}} \approx 13\,\mathrm{eV}$ in a fully ionized beryllium at $\rho \approx 0.5\,\mathrm{g/cm^3}$. As a result, the Coulomb logarithm – hence the stopping power – increases from $L = 7.4$ to 9.0, i.e. by 20%.

An upper estimate for the role of the non-equilibrium effective charge can be obtained by performing two computer runs for identical converter conditions: one with the cold equilibrium value of $Z_{\mathrm{eff}} = Z_{\mathrm{eff}}(v_{\mathrm{bi}})$ given by the corresponding empirical formula, and another with Z_{eff} fixed along the trajectory at its highest possible value ($Z_{\mathrm{eff}} \approx 77$ for the 10 GeV Bi ions). In this way we find that the additional reduction of $\langle \rho l \rangle_{\mathrm{con}}$ caused by this effect does not exceed 10%.

In general, as the target material undergoes ionization, the relative increase of the Coulomb logarithm L in high-Z elements is larger than in low-Z ones. Hence, even a thin cover of gold can shorten considerably the ion path in beryllium behind it. For the planar configuration shown in Fig. 5, where $\langle \rho l \rangle_{\mathrm{cw}} = 0.029\,\mathrm{g/cm^2}$, we calculate the following ranges of 10 GeV Bi ions in beryllium:

cold: $\langle \rho l \rangle_{\mathrm{con}} = 0.116\ \mathrm{g/cm^2}$,

hot: $\langle \rho l \rangle_{\mathrm{con}} = 0.077\ \mathrm{g/cm^2}$.

Here the cold value was calculated before the turn-on of the ion pulse ($t = 0$), whereas the hot one at the end of the pulse ($t = 22\,\mathrm{ns}$). One sees that the combined action of the effects (1) and (3) reduces $\langle \rho l \rangle_{\mathrm{con}}$ by a factor of 1.5, which means that these two effects contribute almost equally to the shortening of $\langle \rho l \rangle_{\mathrm{con}}$.

The process of range shortening in the expanding converter is illustrated in Fig. 5. Initially, the combined thickness of the beryllium converter and its gold cover is slightly below the cold range of the Bi ions. However, after $t \approx 8\,\mathrm{ns}$ the ions are fully stopped inside the converter. The ion penetration front recedes with respect to the mass coordinate, but its position in space remains almost fixed because of the hydrodynamic expansion of the converter. This feature is quite beneficial for maintaining the symmetry of capsule irradiation in the "octopus" target: as the converter material expands and spills out of the converter pockets, the position of the X-ray emitting region can be kept more or less fixed in space. Our calculations demonstrate that the effect of range shortening is of just the right magnitude to be employed for this purpose. In targets with two-sided irradiation and radiation screens the effect of range shortening can be utilized to minimize the beam losses associated with the non-1-D expansion of the converters.

6. Conclusion

Our main conclusion is that the minimum ion beam energy required to obtain thermonuclear

ignition by using the HIDIF driver should be close to 4 MJ. This is roughly twice as much as the NIF laser energy [3]. Hence, while offering good prospects for fusion energy production, a heavy ion driver based on a RF linac and vacuum ballistic focusing does not appear as a promising option for an ignition facility.

This conclusion has been reached by considering relatively simple hohlraum designs. Although the efficiency of the "octopus" target is difficult to improve (because of the large total converter mass involved), one could, in principle, bring the driver energy significantly down in the case of two-sided irradiation by assuming a tighter hohlraum with a more complex arrangement of the radiation screens [13]. Static view factor calculations become of little value in such a case, and even with the integrated 2-D radiation hydrodynamics simulations it is difficult to obtain high-confidence results because of the sensitivity of the target performance to minor details in the hohlraum design.

Acknowledgements

We appreciate many stimulating discussions with I. Hofmann, D. Koshkarev and J. Meyer-ter-Vehn. One of the authors (M.B.) acknowledges financial support from the INTAS under the contract No. 93-2571 and from the ITSC under the contract No. 154.

References

[1] I. Hofmann, R. Bär, R. Bock, H. Eickhoff, G. Franchetti, R.W. Hasse, R.W. Müller, U. Oeftiger, G. Rumolo, P. Spiller, High Energy Density in Matter Produced by Heavy Ion Beams, Report GSI-97-08, 1997, p. 33.
[2] I. Hofmann, Nucl. Instr. and Meth. A 415 (1998) 11.
[3] J. Lindl, Phys. Plasmas 2 (1995) 3933.
[4] T.R. Dittrich, S.W. Haan, S. Pollaine, A.K. Burnham, G.L. Strobel, Fusion Technol 31 (1997) 402.
[5] A. Djaoui, Phys. Plasmas 3 (1996) 4677.
[6] M. Basko, Phys. Plasmas 3 (1996) 4148.
[7] K.-J. Lutz, Dreidimensionale Simulationen des Strahlungstransportes in Schwerionenfusionstargets, Inaugural Dissertation, Universität Frankfurt am Main, November 1997.
[8] D.D.-M. Ho, J.D. Lindl, M. Tabak, Nucl. Fusion 34 (1994) 1081.
[9] M.M. Basko, M.D. Churazov, D.G. Koshkarev, Fusion Eng. Des. 32-33 (1996) 73.
[10] M.M. Basko, Nucl. Fusion 30 (1990) 2443.
[11] S.P. Ahlen, Rev. Mod. Phys. 52 (1980) 121.
[12] T. Peter, J. Meyer-ter-Vehn, Phys. Rev. A 43 (1991) 2015.
[13] R. Ramis, J.J. Honrubia, J. Meyer-ter-Vehn, J. Ramirez, A.R. Piriz, J. Sanz, L.F. Ibañez, M.M. Sanchez, M. de la Torre, Nucl. Instr. and Meth. A 415 (1998) 93.